ELASTIC REGISTRATION OF HIGH-RESOLUTION 3D PLI DATA OF THE HUMAN BRAIN

S. Ali[⋆] *K. Rohr*[⋆] *M. Axer*[†] *D. Gräßel*[†] *P. Schlömer*[†] *K. Amunts*[†] *R. Eils*[⋆] *S. Wörz*[⋆]

[⋆]Dept. of Bioinformatics and Functional Genomics, Biomedical Computer Vision Group, BIOQUANT, IPMB, University of Heidelberg and German Cancer Research Center (DKFZ), Germany
[†]Institute of Neuroscience and Medicine1, Research Centre Jülich, Jülich, Germany

ABSTRACT

We introduce a new approach for the elastic registration of high-resolution 3D polarized light imaging (3D PLI) data of histological sections of the human brain. For accurate registration of different types of 3D PLI modalities, we propose a novel intensity similarity measure that is based on a least-squares formulation of normalized cross-correlation. Moreover, we present a fully automatic registration pipeline for rigid and elastic registration of high-resolution 3D PLI images with a blockface reference including a preprocessing step. We have successfully evaluated our approach using manually obtained ground truth for five sections of a human brain and experimentally compared it with previous approaches. We also present experimental results for 60 brain sections.

Index Terms— 3D PLI, Elastic registration, Human brain

1. INTRODUCTION

The study of the connectome of the human brain is an important topic in neuroscience (e.g., [1]). Main contributions come from electron microscopy, optical microscopy, and diffusion Magnetic Resonance Imaging (MRI). However, each modality is only suited to brain structures in its range of resolution, which either limits the sample size, the number of subjects, or the investigated anatomical features. Diffusion MRI represents to date the only solution to image whole brain connectivity [2], but at the expense of resolution, i.e., reconstructing individual fibers or small fiber bundles is not feasible. To enable whole brain connectivity analysis with much higher resolution, a technique using polarized light referred to as 3D PLI has been utilized for imaging unstained histological brain sections [3]. 3D PLI achieves an image resolution of $64\,\mu m$ using a large area polarimeter, it provides good fiber/non-fiber contrasts for entire human brain sections, and it obtains local *3D fiber orientation vectors* that are essential for determining the 3D fiber architecture. In this work, we utilize histological images of human brain sections with a thickness of $70\,\mu m$. During sectioning, a so-called blockface (BF) image was obtained for each brain section. The stack of reconstructed BF images [4] serves as undistorted reference. Exemplarily, Fig. 1 shows a BF image (left) and a corresponding 3D PLI image (right). With 3D PLI, different types of high-resolution ($64\,\mu m$ pixel size) image modalities are acquired (see Fig. 2): A *light reflectance* image, a *transmittance* image representing light extinction, a *retardation* image showing the tissue birefringence, as well as a *direction* and an *inclination* image giving the local 3D fiber orientation. Unfortunately, due to the tissue sectioning process the 3D spatial coherence between 2D sections is lost (i.e., the sections are arbitrarily positioned and oriented). Moreover, the sectioning process inevitably introduces significant distortions and local tissue deformations as well as partly severe artifacts such as fissures, folds, and gaps. Therefore, linear and non-linear (elastic) registration is required to obtain a 3D reconstruction of high-resolution 3D PLI data. Regarding the registration of *3D PLI data*, only little work can be found [5, 6]. In [5], a relatively small region of a different brain was considered where the 3D PLI data has a coarser (isotropic) resolution of $100\,\mu m$ (such thicker sections are less prone to sectioning artifacts). In contrast, [6] considered 3D PLI data of a rat brain, which is much smaller and has a much simpler structure compared to a human brain. Moreover, both approaches use coarse deformation models that are based on B-splines [6] or a fluid model [5], which do *not* well represent local deformations caused by the sectioning process. Concerning the registration of histological brain sections based on optical imaging, previous work (e.g., [5, 7, 8, 6, 9]) typically follows a common approach where individual sections are first linearly (rigid or affine) registered against a 3D reference (using BF [5, 6], MRI [9], or both [7, 8]), followed by non-linear registration. Different types of non-linear schemes such as diffeomorphic registration (e.g., [9]), free-form deformations using B-splines (e.g., [7, 6]), and local linear grid schemes (e.g., [8]) have

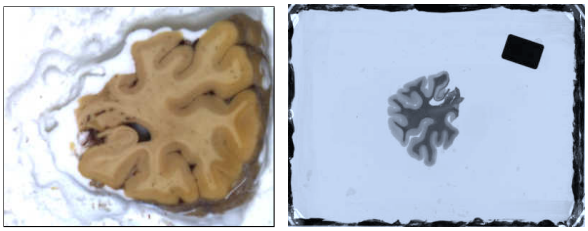

Fig. 1. Section of a temporal lobe of a human brain: Blockface image (left) and 3D PLI transmittance image (right).

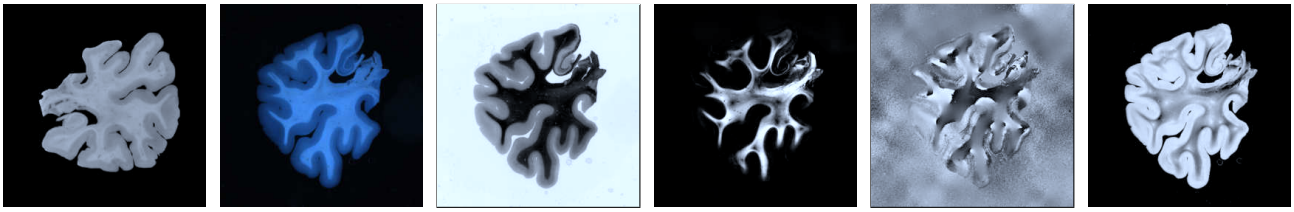

Blockface | Light reflectance | Transmittance | Retardation | Direction | Inclination

Fig. 2. Example section: Blockface image (left) as well as cropped images of different 3D PLI modalities of Fig.1.

been used. However, none of the approaches included a physical deformation model that represents elastic deformations of tissue sections. We introduce a novel approach for the elastic registration of high-resolution 3D PLI data of histological sections of the human brain. The main contribution of our work is two-fold. First, we introduce a novel intensity similarity measure for elastic registration of 3D PLI data with BF images. The similarity measure is based on a least-squares formulation of normalized cross-correlation [10], which we extend for the considered image data. In contrast to [10], where the measure is used for optical flow estimation, we integrate the extended measure in an elastic registration approach based on Gaussian elastic body splines (GEBS) [11]. GEBS have the advantage that they rely on a physical deformation model based on the Navier equation from elasticity theory and thus model local tissue deformations more realistically (e.g., compared to [5, 6]). In comparison to previous multimodal similarity measures used in conjunction with GEBS such as mutual information [12], the proposed measure is more robust, more efficient, and yields more accurate results. Moreover, the measure is suitable both for light reflectance and transmittance 3D PLI modalities. Second, we here present a fully automatic registration pipeline for rigid and elastic registration of high-resolution 3D PLI images with a BF reference including relevant preprocessing (e.g., segmentation). Finally, we have evaluated our approach based on manually obtained ground truth for five sections of a human brain and compared it with previous similarity measures. We also present experimental results for 60 brain sections.

2. ELASTIC 3D PLI REGISTRATION

Below, we first review an elastic registration approach using Gaussian elastic body splines (GEBS) (Sect. 2.1). Then, we introduce the novel intensity similarity measure (Sect. 2.2) and describe the integration into the GEBS approach (Sect. 2.3).

2.1. Intensity-based elastic registration using GEBS

GEBS are based on the Navier equation of elasticity [13]

$$\mu \Delta \mathbf{u} + (\lambda + \mu) \nabla (\operatorname{div} \mathbf{u}) + \mathbf{f} = \mathbf{0} \tag{1}$$

with the deformation vector field $\mathbf{u} = (u, v, w)$, body forces $\mathbf{f}$, and the Lamé constants μ, λ. For 3D Gaussian forces $\mathbf{f}$, an analytic solution of (1) in the form of a matrix-valued basis function has been derived (GEBS, [14]). For intensity-based registration, an energy-minimizing functional J_{GEBS} has been proposed [11] to compute the deformation $\mathbf{u}$ for registration of a source image g_1 with a target image g_2

$$J_{GEBS}(\mathbf{u}) = \tag{2}$$
$$J_{Data,I}\big(g_1, g_2, \mathbf{u}^I\big) + \lambda_I J_I\big(\mathbf{u}, \mathbf{u}^I\big) + \lambda_E\, J_{Elastic}(\mathbf{u})\,,$$

which consists of three terms. Besides $\mathbf{u}$, (2) comprises a second deformation field $\mathbf{u}^I$ which is computed based on the *intensity* information. The first term $J_{Data,I}$ represents an *intensity similarity measure* between the deformed source and target image. In previous work, we used the sum-of-squared intensity differences (SSD) for the monomodal case [11] as well as joint entropy (JE) and mutual information (MI) for the multimodal case [12]. In Sect. 2.2 below, we introduce a new correlation-based measure for GEBS that is well suited for registration of 3D PLI data. The second term J_I *couples* the intensity-based deformation field $\mathbf{u}^I$ with $\mathbf{u}$ using a weighted Euclidean distance (see [11] for details). Finally, the third term $J_{Elastic}$ represents the *regularization* of the deformation field $\mathbf{u}$ based on the elastic energy according to the Navier equation. An efficient way of minimizing J_{GEBS} is to minimize it *alternatingly* w.r.t. $\mathbf{u}^I$ and $\mathbf{u}$ until convergence of the resulting deformation field $\mathbf{u}$ is achieved. For minimization w.r.t. $\mathbf{u}^I$, we developed an efficient strategy for the new similarity measure presented in Sect. 2.3 below. For minimization w.r.t. $\mathbf{u}$, we use the analytic solution derived in [11].

2.2. Intensity similarity measure

A suitable intensity similarity measure for the registration of 3D PLI data with BF images is given by the normalized cross-correlation (NCC, e.g., [15])

$$NCC\,(g_1, g_2) = \frac{1}{N} \sum\nolimits_{\mathbf{x}} \frac{(g_1(\mathbf{x}) - \mu_1) \cdot (g_2(\mathbf{x}) - \mu_2)}{\sigma_1 \sigma_2} \tag{3}$$

where g_1 and g_2 are two images with N pixels each as well as their mean values μ_1 and μ_2, and standard deviations σ_1 and σ_2, respectively. Minimization of $1 - NCC$ yields the optimum zero for $g_1 = g_2$. However, the optimization of this measure is not trivial and computationally expensive, and it is difficult to integrate it in the data term $J_{Data,I}$ in (2). To

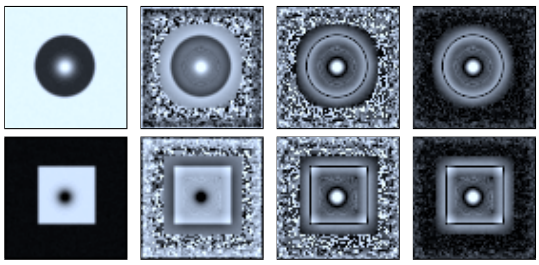

Original $\tilde{g}(\mathbf{x})$ $|\tilde{g}(\mathbf{x})|$ $\breve{g}(\mathbf{x})$

Fig. 3. Example results of the correlation transform $\tilde{g}(\mathbf{x})$ and its extensions $|\tilde{g}(\mathbf{x})|$ and $\breve{g}(\mathbf{x})$ for images of a disk (top) and a square (bottom) with a Gaussian spot in their center.

simplify the integration into the GEBS approach, we reformulate the measure in (3) using the correlation transform (CoT) $\tilde{g}(\mathbf{x})$, which yields a *least-squares* formulation [10]:

$$1 - NCC(g_1, g_2) = \frac{1}{2N} \sum\nolimits_{\mathbf{x}} \left(\tilde{g}_1(\mathbf{x}) - \tilde{g}_2(\mathbf{x})\right)^2 \quad (4)$$

The CoT $\tilde{g}(\mathbf{x})$ (aka standard score, z-score) is given by

$$\tilde{g}(\mathbf{x}) = \left(g(\mathbf{x}) - \mu_g\right)/\sigma_g. \quad (5)$$

For example, Fig. 3 shows the result of the CoT $\tilde{g}(\mathbf{x})$ for images of a disk (top) and square (bottom), both with a Gaussian spot in the center and having roughly inverted contrast. The CoT has been computed using (5) where for each pixel $\mathbf{x}$ the mean μ_g and standard deviation σ_g are computed in a local neighborhood (we used a size of 11×11 pixels). It can be seen in the transformed images that the intensities differ largely between the circle and the square, and that the small amount of image noise present in the original images (hardly visible) is strongly amplified. Thus, $\tilde{g}(\mathbf{x})$ is not directly suitable for the least-squares formulation in (4).

To develop a more suitable similarity measure, we extend the idea of [10] in two ways: First, we use the absolute value $|\tilde{g}(\mathbf{x})|$ of the CoT, which yields a result that is independent of the contrast (Fig. 3). And second, we clip the computed standard deviation below a certain threshold T_σ to avoid division by small values in homogeneous regions, which removes the amplified noise (Fig. 3, right). The extended CoT $\breve{g}(\mathbf{x})$ reads

$$\breve{g}(\mathbf{x}) = \left|g(\mathbf{x}) - \mu_g\right| / \mathrm{clip}\left(\sigma_g, [T_\sigma, \infty]\right), \quad (6)$$

and emphasizes edges and other features like spots independently of the contrast, it is robust against noise, and it is thus well suited for the least-squares formulation in (4).

2.3. Integration and optimization of similarity measure

The data term $J_{Data,I}$ of the new NCC measure is given by:

$$J_{Data,I}(g_1, g_2, \mathbf{u}^I) = \sum\nolimits_{\mathbf{x}} \left(\breve{g}_1(\mathbf{x} + \mathbf{u}^I) - \breve{g}_2(\mathbf{x})\right)^2 \quad (7)$$

For minimization of the overall functional J_{GEBS} w.r.t. $\mathbf{u}^I$, we use a local pixel-wise formulation of $J_{Data,I} + \lambda_I J_I$ as

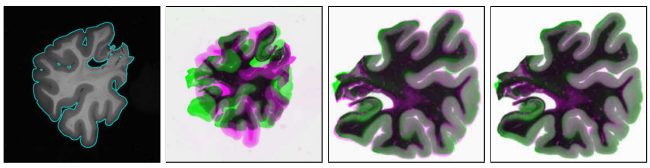

Segmentation COM alignm. Rigid reg. Elastic reg.

Fig. 4. Main steps of 3D PLI registration pipeline.

described in [11]. However, in contrast to [11, 12] we here introduce a Gaussian-weighted region-of-interest (ROI), i.e., $J_{Data,I} + \lambda_I J_I$ reads for a pixel $\mathbf{x}_0$

$$\sum\nolimits_{\mathbf{x} \in ROI} G_\sigma^{2D}\left(\|\mathbf{x} - \mathbf{x}_0\|\right) \left(\breve{g}_1(\mathbf{x} + \mathbf{u}^I) - \breve{g}_2(\mathbf{x})\right)^2 + \lambda_I \|\mathbf{u}^I(\mathbf{x}_0) - \mathbf{u}(\mathbf{x}_0)\| \quad (8)$$

where G_σ^{2D} denotes a 2D Gaussian with standard deviation σ (we used $\sigma = 1$). The reason for using a Gaussian ROI is that $\breve{g}$ yields similar values on both sides of an edge (see Fig. 3 right), which can lead to ambiguous results in local optimization if no neighborhood information is available.

Since (8) comprises only (weighted) squared differences, we use the efficient minimization scheme of Levenberg/Marquardt [16, 17]. The extended CoT of the target image is precomputed before registration, and of the source image is computed once before each minimization step.

3. 3D PLI REGISTRATION PIPELINE

Our fully automatic registration pipeline comprises preprocessing as well as rigid and elastic registration.

Preprocessing For registration of 3D PLI data with BF images (see Fig. 1), localization of the brain within the 3D PLI data is required. To this end, we segment the brain using a two-step refinement approach. First, we apply linear and non-linear noise reduction and multi-level Otsu thresholding [18] with 3 different thresholds, followed by morphological operations and shape filters to remove undesired shapes to obtain a coarse segmentation. Second, we refine the results by using Huang thresholding [19] within an enlarged bounding box of the coarse segmentation. For example, Fig. 4 (left) shows the segmentation result for the 3D PLI section of Fig. 1 (right). Next, we compute the center of mass (COM) of the segmented BF [4] and 3D PLI images, and compute an initial alignment by matching the COMs (see Fig. 4 for a color overlay).

Rigid registration For rigid registration of the initially aligned BF and 3D PLI images, we use the scheme in [20]. Prior to registration we transform the intensities of the BF image to resemble the intensities of the light reflectance 3D PLI image. To initialize the orientation we apply rigid registration to downscaled versions of the images (factor 4) by using 36 different orientations, and choose the result with lowest error. Fig. 4 and Fig. 5 (left) show rigid registration results.

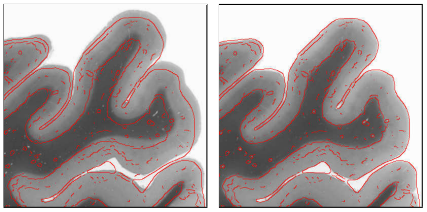

Fig. 5. Rigid (left) and elastic (right) registration result overlaid with edges of the BF image for a ROI of results in Fig. 4.

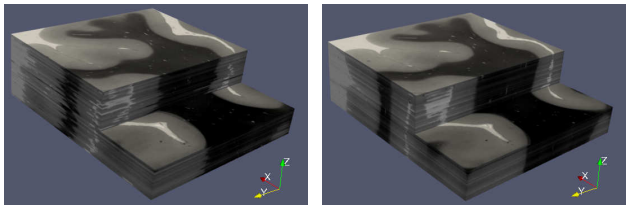

Fig. 6. Rigid (left) and elastic registration (right) of 60 consecutive sections of 3D PLI data of a human brain.

Elastic registration After rigid registration, we use elastic registration to compensate local deformations caused by the sectioning process. We use the GEBS approach described in Sect. 2.1 with the novel NCC-based similarity measure presented in Sections 2.2 and 2.3. To enable registration of larger deformations, we use four multi-resolution levels, and to ensure realistic deformations we verify that the Jacobian remains positive. As source image, we choose either the light reflectance or transmittance 3D PLI image. The final deformation field is then applied to all 3D PLI modalities (see Fig. 2). Figs. 4 and 5 (right) show elastic registration results.

4. EXPERIMENTAL RESULTS

We have evaluated our new approach and the registration pipeline using five sections of a human brain each of $64\mu m$ pixel size. Ground truth correspondences between the 3D PLI data and the BF reference have been manually defined by two experts (on average 76 correspondences per section). Table 1 shows the target registration error (TRE) for COM alignment, rigid registration, and elastic registration using either the transmittance or the light reflectance 3D PLI modality as source image. We also compared our new NCC measure with previous joint entropy (JE) and mutual information (MI) [12].

The mean TRE of *rigid* registration is 10.68 pixels, while *elastic* registration yields the best results using the new NCC measure with mean errors of 3.79 and 3.64 pixels for transmittance and light reflectance images, respectively. These values are even below the interobserver variability of 4.53 pixels. In comparison, JE and MI yield larger TREs for all single sections. Using JE, it was not possible to obtain proper results for light reflectance images. Moreover, we have successfully applied our registration pipeline to 60 consecutive sections of a human brain. Fig. 6 shows a 3D visualization of the aligned sections using rigid registration (left) and elastic registration with NCC (right). It can be seen that using elastic registration the sections including fine brain structures are well aligned.

5. CONCLUSIONS

We have introduced a new approach for the elastic registration of high-resolution 3D PLI data of histological sections of the human brain. We proposed a novel intensity similarity measure that extends a previous least-squares formulation of normalized cross-correlation. Moreover, a fully automatic registration pipeline, which comprises preprocessing as well as rigid and elastic registration of 3D PLI data with a BF reference is presented. We have successfully evaluated our approach using manually obtained ground truth correspondences for five sections of a human brain and experimentally compared it with previous approaches. We also presented experimental results for 60 brain sections.

Acknowledgment

This work was supported by the Helmholtz Association through the Helmholtz Portfolio theme "Supercomputing and Modeling for the Human Brain".

TRE in pixels (mean±stdDev)	3D PLI section #1	#2	#3	#4	#5	Mean
COM alignment	573.91±225.	529.92±224.	517.40±210.	527.02±236.	553.71±219.	540.39±223.
Rigid registration	11.98±6.53	6.85±4.77	8.16±5.04	13.14±8.55	13.25±7.19	10.68±6.42
Source: Transmittance image						
Elastic: JE [12]	7.05±3.65	3.59±2.18	4.81±3.16	7.75±9.82	8.14±7.60	6.27±5.28
Elastic: MI [12]	6.71±5.31	3.74±3.01	4.04±2.53	5.03±3.78	6.96±6.38	5.30±4.20
Elastic: New NCC measure	**4.27±3.01**	**2.93±1.83**	**3.88±2.30**	**3.67±2.28**	**4.20±3.37**	**3.79±2.56**
Source: Light reflectance image						
Elastic: JE [12]	19.26±11.4	17.07±6.49	8.64±6.49	17.57±7.79	16.73±9.37	15.85±8.30
Elastic: MI [12]	5.04±3.27	4.32±3.65	4.13±2.52	5.00±4.94	6.38±6.12	4.98±4.10
Elastic: New NCC measure	**4.19±3.07**	**2.92±1.85**	**3.67±2.12**	**3.31±2.30**	**4.10±3.72**	**3.64±2.61**
Interobserver variability	5.29±6.45	6.53±9.30	4.47±5.21	3.48±3.59	2.88±3.31	4.53±5.57

Table 1. Evaluation of registration pipeline and comparison of different similarity measures using five 3D PLI brain sections.

6. REFERENCES

[1] G. Deco and M. L. Kringelbach, "Great expectations: using whole-brain computational connectomics for understanding neuropsychiatric disorders," *Neuron*, vol. 84, no. 5, pp. 892–905, 2014.

[2] M. Bastiani and A. Roebroeck, "Unraveling the multiscale structural organization and connectivity of the human brain: the role of diffusion MRI," *Frontiers in Neuroanatomy*, vol. 9, no. 77, 2015.

[3] M. Axer, D. Gräßel, M. Kleiner, J. Dammers, T. Dickscheid, J. Reckfort, T. Hütz, B. Eiben, U. Pietrzyk, K. Zilles, and K. Amunts, "High-resolution fiber tract reconstruction in the human brain by means of three-dimensional polarized light imaging," *Frontiers in Neuroinformatics*, vol. 5, no. 34, 2011.

[4] M. Schober, P. Schlömer, M. Cremer, H. Mohlberg, A.-M. Huynh, N. Schubert, M.E. Kirlangic, K. Amunts, and M. Axer, "Reference Volume Generation for Subsequent 3D Reconstruction of Histological Sections," in *Proc. Workshop Bildverarbeitung für die Medizin (BVM'15)*, H. Handels, T.M. Deserno, H.-P. Meinzer, and T. Tolxdorff, Eds., Lübeck, Germany, March 2015, Informatik aktuell, pp. 143–148, Springer Berlin Heidelberg.

[5] C. Palm, M. Axer, D. Gräßel, J. Dammers, J. Lindemeyer, K. Zilles, U. Pietrzyk, and K. Amunts, "Towards ultra-high resolution fibre tract mapping of the human brain - registration of polarised light images and reorientation of fibre vectors," *Frontiers in Human Neuroscience*, vol. 4, no. 9, 2010.

[6] N. Schubert, M. Axer, M. Schober, A. Huynh, M. Huysegoms, N. Palomero-Gallagher, J. G. Bjaalie, T. B. Leergaard, M. E. Kirlangic, K. Amunts, and K. Zilles, "3D reconstructed cyto-, muscarinic m2 receptor, and fiber architecture of the rat brain registered to the waxholm space atlas," *Frontiers in Neuroanatomy*, vol. 10, no. 51, 2016.

[7] J. Lebenberg, A.-S. Hérard, A. Dubois, J. Dauguet, V. Frouin, M. Dhenaina, P. Hantraye, and T. Delzescaux, "Validation of MRI-based 3D digital atlas registration with histological and autoradiographic volumes: An anatomofunctional transgenic mouse brain imaging study," *NeuroImage*, vol. 51, pp. 1037–1046, 2010.

[8] K. Amunts, C. Lepage, L. Borgeat, H. Mohlberg, T. Dickscheid, M.-E. Rousseau, S. Bludau, P.-L. Bazin, L.B. Lewis, A.-M. Oros-Peusquens, N.J. Shah, T. Lippert, K. Zilles, and A.C. Evans, "BigBrain: An Ultrahigh-Resolution 3D Human Brain Model," *Science*, vol. 340, pp. 1472–1475, 2013.

[9] P. Majka and D.K. Wójcik, "Possum–A Framework for Three-Dimensional Reconstruction of Brain Images from Serial Sections," *Neuroinformatics*, vol. 14, no. 3, pp. 265–278, 2016.

[10] M. Drulea and S. Nedevschi, "Motion Estimation Using the Correlation Transform," *IEEE Trans. on Image Processing*, vol. 22, no. 8, pp. 3260–3270, 2013.

[11] S. Wörz and K. Rohr, "Spline-Based Hybrid Image Registration using Landmark and Intensity Information based on Matrix-Valued Non-Radial Basis Functions," *Internat. J. of Computer Vision*, vol. 106, no. 1, pp. 76–92, 2014.

[12] A. Biesdorf, S. Wörz, H.-J. Kaiser, C. Stippich, and K. Rohr, "Hybrid Spline-Based Multimodal Registration using Local Measures for Joint Entropy and Mutual Information," in *Proc. Twelfth Internat. Conf. on Medical Image Computing and Computer-Assisted Intervention (MICCAI'09)*, G.Z. Yang, D.J. Hawkes, D. Rueckert, A.J. Noble, and C.J. Taylor, Eds., London, UK, Sept. 2009, vol. 5761 of *Lecture Notes in Computer Science*, pp. 607–615, Springer Berlin Heidelberg.

[13] P.C. Chou and N.J. Pagano, *Elasticity – Tensor, Dyadic, and Engineering Approaches*, Dover Publications, Inc., Mineola, NY/USA, 1992.

[14] J. Kohlrausch, K. Rohr, and H.S. Stiehl, "A New Class of Elastic Body Splines for Nonrigid Registration of Medical Images," *J. of Mathematical Imaging and Vision*, vol. 23, no. 3, pp. 253–280, 2005.

[15] A. Roche, G. Malandain, and N. Ayache, "Unifying Maximum Likelihood Approaches in Medical Image Registration," *Int. J. Imaging Systems Technolog.*, vol. 11, pp. 71–80, 2000.

[16] D. Marquardt, "An Algorithm for Least-Squares Estimation of Nonlinear Parameters," *J. of the Society for Industrial and Applied Mathematics*, vol. 11, no. 2, pp. 431–441, 1963.

[17] W.H. Press, B.P. Flannery, S.A. Teukolsky, and W.T. Vetterling, *Numerical Recipes in C*, Cambridge University Press, Cambridge, UK, 1992.

[18] N. Otsu, "A Threshold Selection Method from Grey Level Histograms," *IEEE Trans. on Systems, Man and Cybernetics*, vol. 9, no. 1, pp. 62–66, 1979.

[19] L.-K. Huang and M.-J.J. Wang, "Image Thresholding by Minimizing the Measures of Fuzziness," *Pattern Recognition*, vol. 28, no. 1, pp. 41–51, 1995.

[20] P. Thévenaz, U.E. Ruttimann, and M. Unser, "A Pyramid Approach to Subpixel Registration based on Intensity," *IEEE Trans. on Image Processing*, vol. 7, no. 1, pp. 27–41, 1998.